Iraqi journal of Bioscience and Biomedical
Published Online First: 31/December/2025
p-ISSN: 3007-5491 / e-ISSN:3007-5505

Synthesis, and Docking Study of Novel Mannich-Base Triazole Derivatives as Potent Inhibitors of β-Tubulin

Wahad K. Kareem[1], Nasreen R. Jber*[2], Ahmed Al-Ani[3]

[1,2,3] Chemistry Department, College of Science, Al-Nahrain University, Baghdad, Iraq.

*Corresponding Author: nasreen.jber@nahrainuniv.edu.iq

Received ;10/10/2025, Accepted :21/10/2025, Published :31/12/2025.

Abstract

Tubulin inhibitors cure aggressive breast tumors, particularly triple-negative. They disrupt cell-dividing microtubules to halt cancer cell proliferation. Triazole heterocyclic scaffolds are popular in pharmaceutical science owing to their various biological activity and drug-like characteristics. Study examines synthesis, FTIR and 1H-NMR characterisation, and molecular docking of Mannich base triazole derivatives targeting the β-tubulin binding site (PDB ID: 3O2F), a proven breast cancer therapeutic focus. Isatin was condensed with piperazine and formaldehyde, then imines were formed by utilizing 4-aminobenzoic acid. Due to increased solubility and binding selectivity, synthesized derivatives (A1, A2, A3, F) were structurally optimized using DFT (B3LYP/6-31G) and assessed using MOE tool. Docking studies showed that all of the compounds had larger binding affinities than PU-H54 (–7.17 kcal/mol), with compound F having the highest score of –9.23. These findings are encouraging, but further in vitro and in vivo testing is needed to determine their medicinal potential.

Keywords: Breast cancer, Triazole, Mannich base, Molecular docking.

Introduction

Tubulin inhibitors are chemotherapeutic medicines used to treat aggressive breast cancers including triple-negative. They stop cancer cell growth by breaking microtubules, which divide cells. Triazoles are five-membered heterocyclic molecules having three nitrogen atoms in a 1,3,4-, 13,5-, or 1,2,4-ring [1]. Due to their unique electrical characteristics, stability, and ability to engage in numerous chemical processes, triazole derivatives are preferred scaffolds in medicinal chemistry [2]. Most study has concentrated on their synthesis and biological testing. Because their structural properties allow varied biological target interactions, scientists have investigated these chemicals as possible anticancer medicines [3] Recent research shows that these heterocycles, especially the 1,3,4-triazole isomer, are often used in therapeutic candidates because their bioisosteric similarity to amides and esters improves lipophilicity and metabolic stability [4]. Adding them to bioactive compounds increases selectivity and effectiveness, especially in targeting cancer cell lines like MCF-7, a common estrogen receptor- positive breast cancer treatment [5].

Iraqi journal of Bioscience and Biomedical
Published Online First: 31/December/2025
p-ISSN: 3007-5491 / e-ISSN:3007-5505

Triazoles are important in medicine due to their synthetic flexibility and pharmacological versatility [6]. These include antibacterial, antifungal, antiviral, anti-inflammatory, and most importantly, anticancer [7]. ecause of triazole-containing chemicals' capacity to disrupt cancer pathways, their anticancer potential has garnered attention [8]. In cancer cells, they decrease tubulin polymerization, alter kinase activity, and trigger apoptosis. If triazole derivatives are rationally developed with suitable substituents, their interaction with cancer cell molecular targets may be tuned to enhance treatment effects [9].

Breast tumors is a primary cause of mortality for women globally. Hormone-responsive subtypes are frequent, and laboratory studies have explored their physiology [10]. esearchers have frequently used this cell line to test new chemotherapeutic drugs' cytotoxicity [11]. Triazole compounds have shown promising antiproliferative actions against MCF-7 cells, frequently outperforming standard medicines [12]. Due to their ability to cause cell cycle arrest, ROS generation, and mitochondrial-mediated apoptosis [13]. Certain 1,3,4-triazole-based hybrids conjugated with moieties such quinolines, coumarins, or sulfonamides exhibit increased cytotoxicity, indicating synergistic effects that might be used in future drug design [14].

Triazole derivatives are prepared via the Mannich process, especially when functionalizing heterocycles to improve biological activities [15]. The Mannich process creates diverse compounds with increased solubility, reactivity, and target selectivity by adding aminomethyl groups to triazole rings [16]. The drugs' pharmacokinetic characteristics and biological interactions generally improve after these adjustments. In the medical field, Mannich-based triazole have shown promising activity against various diseases, especially cancer [17]. Several derivatives exhibit potent cytotoxicity against breast cancer (such as, MCF-7 cells), where the Mannich base moiety can facilitate better binding to cellular targets or improve drug delivery across membranes [18].

This study aimed to bridge anticancer chemistry and computational modeling. This study seeks to design, develop, and assess novel Mannich base derivatives containing triazole rings as potential β-tubulin inhibitors for breast cancer therapy. So, synthesis novel triazole derivatives and characterize them by FTIR and ^{1}H-NMR. Ultimately, the project aspires to deliver molecular scaffolds for targeted therapy against MCF-7 cell lines, contributing to more effective and selective anticancer drug development.

Materials and Methods

Materials

The materials, such as Isatin, piperazine, tetrahydrofuran, chloroform and glacial acetic acid, were obtained from Sigma Aldrich. In contrast, 4-aminobenzoic acid and formaldehyde from Merck and the absolute ethanol (99%) were obtained from BDH that used to synthesize triazole derivatives.

Methodology

Synthesis of Mannich base (1)

Isatin (3.52 g, 0.02 mol) was first dissolved in 35 mL of tetrahydrofuran. Subsequently, piperazine (1.032 g, 0.01 mol) was added, followed by the gradual addition of 12 mL of aqueous formaldehyde solution. The reaction mixture was left at room temperature for 1 hour, then heated on a steam bath for 20

Iraqi journal of Bioscience and Biomedical
Published Online First: 31/December/2025
p-ISSN: 3007-5491 / e-ISSN:3007-5505

minutes. After heating, it was stored at 4 °C for 48 hours to ensure completion. The solid product (1) was obtained and purified by recrystallization from a mixture of ethanol and chloroform [19].

Synthesis of Imine derivative (2)

A solution of derivative 1 (0.1 mol) in 10 mL of absolute ethanol was prepared, and three drops of glacial acetic acid were added to activate the carbonyl group. Then, 4-aminobenzoic acid (0.2 mol) was introduced, and the mixture was refluxed at 80 °C for 4 hours. Under these acidic conditions, condensation proceeded efficiently, producing the desired product as a precipitate [20].

Synthesis of Triazole Derivatives (5)

The derivative (3) was synthesized by the esterification of the carboxylic group of vanillic acid (2) using thionyl chloride ($SOCl_2$) in cold ethanol. Ethanol vanillate was reacted with hydrazine hydrate to yield a hydrazide derivative 4, which subsequently reacted with carbon disulphide in the presence of potassium hydroxide (KOH) to form a potassium dithiocarbamate derivative 5, as shown in Scheme 1.

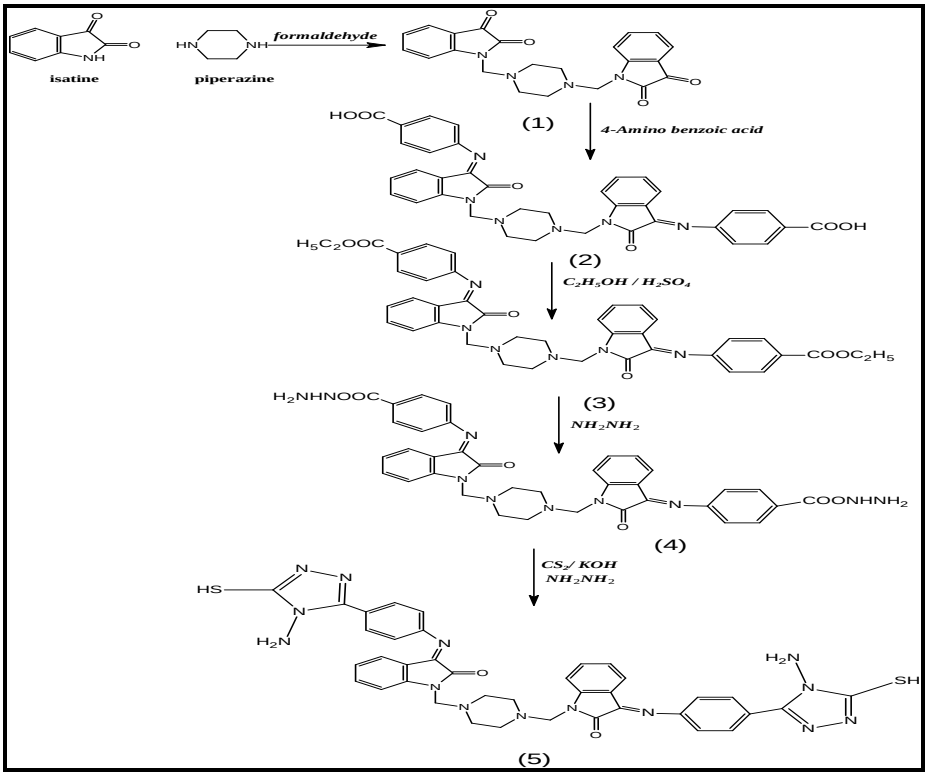

Scheme 1. Routes synthesis of derivative (5).

Synthesis of Triazole Derivatives (A1-A3)

The derivatives (4) (0.001 mole) were dissolved in absolute ethanol (20 mL) with potassium hydroxide (2 mol, 1.38 g), followed by the addition of (0.002 mole) of alkyl halide, such as methyl, ethyl, and propyl. The mixture was refluxed for 24 hours at 80°C. The resultant goods were filtered, as shown in Figure 1.

Iraqi journal of Bioscience and Biomedical
Published Online First: 31/December/2025
p-ISSN: 3007-5491 / e-ISSN:3007-5505

Synthesis of Triazole Derivatives (F)

Compound (4) (0.01 mol) and 4-hydroxybenzaldehyde (0.02 mol) are each dissolved in 25 mL of absolute ethanol and refluxed on a water bath for several hours. During the reflux, 3–4 drops of glacial acetic acid are added to promote condensation. Once heating is complete, the reaction mixture is poured into ice-cold water, leading to the precipitation of the product. The solid is separated by filtration, washed thoroughly with cold water, and dried. The crude material has then been purified by recrystallisation from hot ethanol to obtain the final product in a pure form [21], as shown in Figure 1.

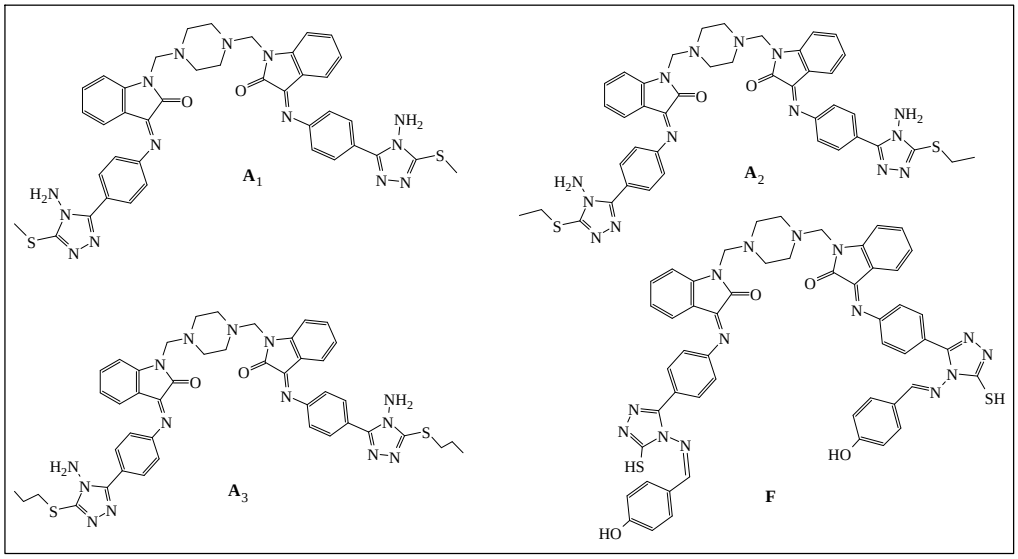

Figure 1. Chemical Structure of synthesized triazole derivatives via draw chemdraw ultra (8.0).

Molecules Library Preparation

Derivatives A1, A2, A3, and F have been synthesized and prepared for molecular docking analysis. Their 3D structures were built using Chemdraw Ultra 12.0 (https://chemdraw-pro.software.informer.com/12.0/) and refined through energy minimization. Initial optimization was performed with the semi-empirical AM1 method in Hyperchem 8.08, followed by density functional theory at the B3LYP/6-31G level to obtain stable conformations. Default convergence settings for maximum force, RMS force, maximum displacement, and RMS displacement were satisfied. Vibrational frequency calculations produced positive values, confirming the structural stability of all ligands [22]. The optimized structures were compiled into a single database using MOE software (Molecular Operating Environment, 2022) for ligand affinity studies, as shown in Figure 1. In addition, Figure 2 presents a schematic overview of the docking workflow, including ligand analysis and reactivity assessment.

Iraqi journal of Bioscience and Biomedical
Published Online First: 31/December/2025
p-ISSN: 3007-5491 / e-ISSN:3007-5505

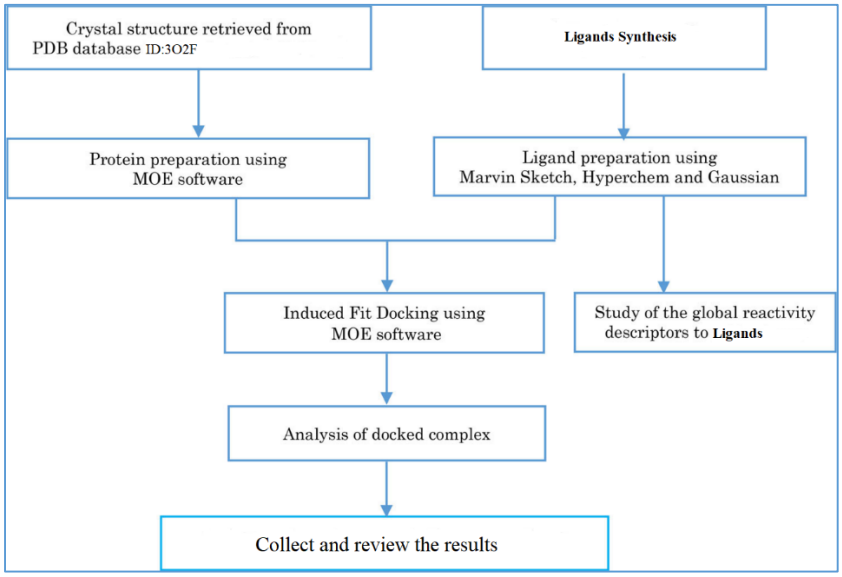

Figure 2. Schematic representation of the docking procedure, analysis of drugs and reactivity.

The crystal structure of the GRP94 N-domain bound to PU-H54 (PDB ID: 3O2F) (Figure 3) was obtained from the Protein Data Bank. A water molecule was retained in the active site to support hydrogen bonding. Missing X-ray bonds were corrected, and hydrogen atoms were added during protein preparation [23]. The 3O2F protein represents the crystal structure of human β-tubulin in complex with paclitaxel, a microtubule-stabilizing agent cornerstone in breast cancer chemotherapy. Microtubules are essential for cell division, and their dynamics are frequently dysregulated in breast cancer cells, leading to uncontrolled proliferation. Paclitaxel binds specifically to the taxane site on β-tubulin, as shown in the 3O2F structure, stabilizing microtubules and inhibiting mitosis. This mechanism is exploited clinically to suppress the growth of rapidly dividing breast cancer cells. The 3O2F model thus serves as a valuable structural template for in silico screening and rational drug design of new microtubule-targeting agents, which could enhance the efficacy or safety of breast cancer therapy [24].

Iraqi journal of Bioscience and Biomedical
Published Online First: 31/December/2025
p-ISSN: 3007-5491 / e-ISSN:3007-5505

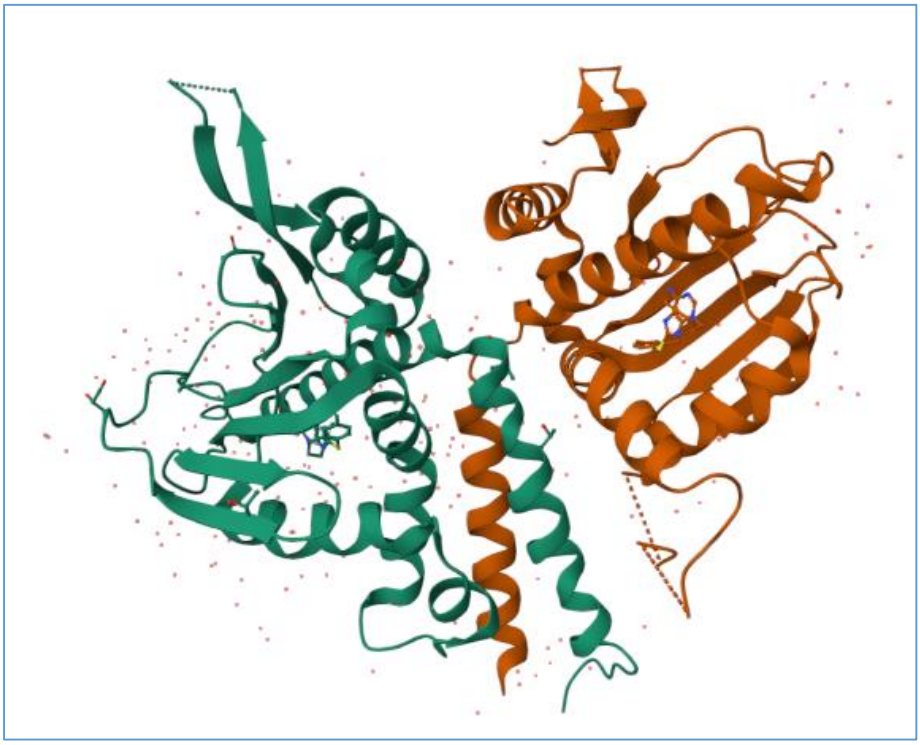

Figure 3. Crystal structures of the 3O2F protein which obtained from PDH website of proteins.

Ligand–Protein molecular docking

Docking and scoring calculations were carried out using MOE software (Molecular Operating Environment, 2022). The crystal structure of the GRP94 N-domain complexed with PU-H54 (PDB ID: 3O2F, 2.50 Å resolution) was obtained from the Protein Data Bank. Resolutions of 1.4–2.5 Å are suitable for docking. Validation commonly requires RMSD values near 2 Å and binding energies of ≤ -7 kcal/mol [23].

The evaluation of cytotoxicity for the inhibitor was conducted using the MTT Assay on the breast cancer cell line MCF-7

The cytotoxicity of the synthesized derivatives was measured using the MTT ready-to-use kit (Intron Biotech).

A. Kit components:
MTT solution, 3-(4,5-dimethylthiazol-2-yl)-2,5-diphenyl tetrazolium bromide (MW = 414), supplied as 1 mL × 10 vials

Solubilization solution, supplied as 50 mL × 2 bottles.

Iraqi journal of Bioscience and Biomedical
Published Online First: 31/December/2025
p-ISSN: 3007-5491 / e-ISSN:3007-5505

B. Procedure

Assay included seeding MCF-7 cells (4.5×10^5) on plates with 200 µL of complete media per well. After sealing with sterile parafilm, plates were gently mixed and incubated at 37 °C with 5% CO_2 for 24 hours. After incubation, the medium was replenished with 200 µL of a two-fold serial dilution of the synthesized derivatives (0, 20, 40, 80, 160, 320 µg/mL). Three times each concentration and control were tested. Plates were incubated at 37 °C with 5% CO_2 for 24 hours. After treatment, 10 µL MTT solution was applied to each well. We incubated plates for 4 more hours under the same circumstances. The media was carefully removed, 100 µL of DMSO solubilization solution was added to each well, and incubated for 5 min. An ELISA reader (Bio-Rad, Germany) measured absorbance at 575 nm.

Results

Characterization

The FTIR and 1H-NMR spectra of compounds A1–A3 and F support their structural designations. Compound A1 exhibits FTIR absorptions at 3412 and 3275 cm^{-1}, indicating primary amine group stretching. The band at 3041 cm^{-1} represents aromatic C–H stretching, whereas peaks at 2924 and 2854 cm^{-1} represent aliphatic stretching. A high signal at 1639 cm^{-1} indicates C=N stretching, whereas absorption at 1257 cm^{-1} indicates C–N stretching. A 1H-NMR spectrum confirms these observations. Due to ring symmetry, aromatic protons show as multiplets at δ 7.3-7.7 ppm. The amino group is confirmed by a singlet at δ 6.2 ppm, whereas methylene protons coupled to the nitrogen atom in isatin resonate at δ 3.9-4.4 ppm.

Compound A2 exhibits primary amine stretching FTIR bands at 3381 and 3348 cm^{-1}. Aliphatic C–H stretching occurs at 2960 and 2933 cm^{-1}. A band at 1670 cm^{-1} indicates C=N stretching, whereas another at 1274 cm^{-1} indicates C–N stretching. The 1H-NMR spectra shows aromatic multiplets at δ 7.0–7.8 ppm. A singlet at δ 6.2 ppm indicates amino protons. Methyl protons are indicated by triplet signals at δ 1.2-1.3 ppm, whereas methylene groups near the nitrogen atom resonate at δ 4.0-4.1 ppm. The FTIR spectrum of compound A3 shows absorption peaks at 3419 and 3413 cm^{-1}, confirming the presence of primary amine groups. Bands at 2979 and 2854 cm^{-1} correspond to aliphatic C–H stretching, while 1660 cm^{-1} and 1257 cm^{-1} are associated with C=N and C–N stretching, respectively. The ^{1}H-NMR spectrum displays aromatic multiplets between δ 7.5–7.8 ppm. A singlet at δ 6.5 ppm corresponds to amino protons. Triplet signals appear at δ 1.20–1.23 ppm for methyl protons, and δ 1.30–1.31 ppm for methylene protons. Additional signals at δ 3.8–3.9 ppm indicate –SCH2 groups. Methylene protons bonded to nitrogen resonate between δ 4.01–4.09 ppm.

Compound F shows distinct FTIR bands: Broad band at 3211 cm^{-1} that could be attributed to O – H stretching and bands at 2754, 1683, 1618 and 1573 and 1271 due to S – H, C = O, CH = N, C = C, C – O stretching, respectively. The ^{1}H-NMR spectrum reveals signals at δ 9.86 belong to phenolic proton – OH. Signals at δ 6.52 belong to proton – NH. Two signals in aromatic region, two doublet at δ 7.50 – 7.81 (24 H) for (disubstituted benzene). Doublet at δ 3.86 – 3.89 for CH_2- (8 -H, piperazine ring). These spectral data confirm that the compounds share an isatin-based structure but differ in side-chain substitutions. The variations in FTIR absorptions and NMR chemical shifts highlight the presence of additional functional groups, strengthening the interpretation of their molecular frameworks, as shown in Figures 4-11.

Iraqi journal of Bioscience and Biomedical
Published Online First: 31/December/2025
p-ISSN: 3007-5491 / e-ISSN:3007-5505

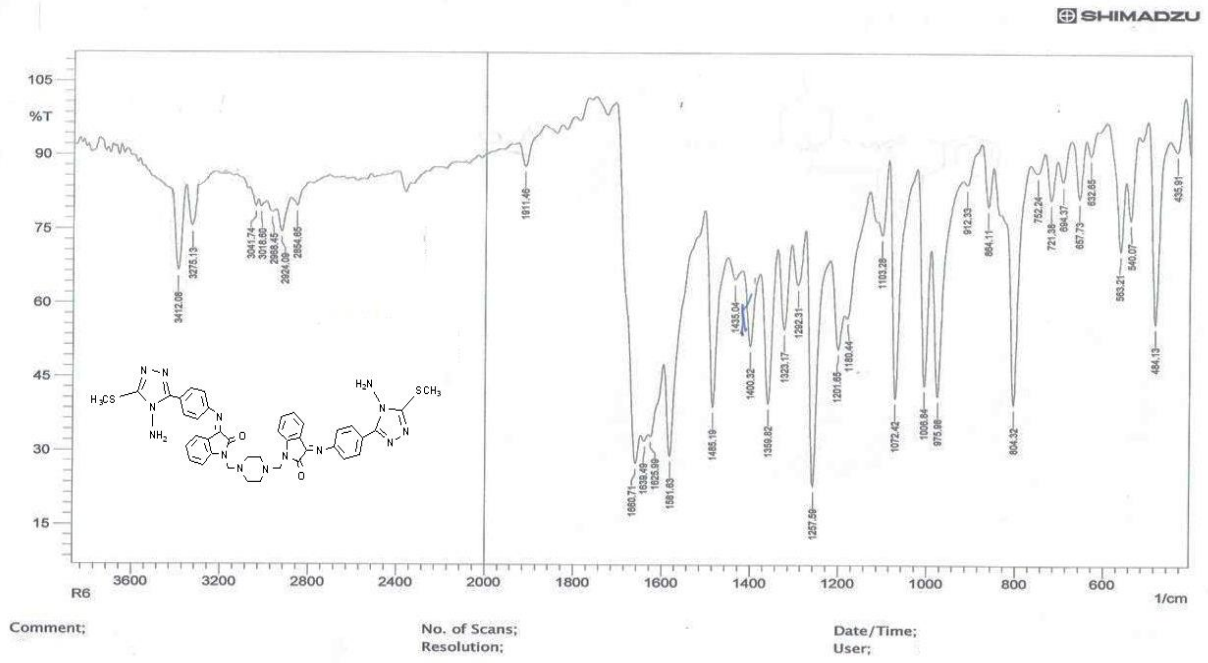

Figure 4. FTIR spectrum of derivative A1.

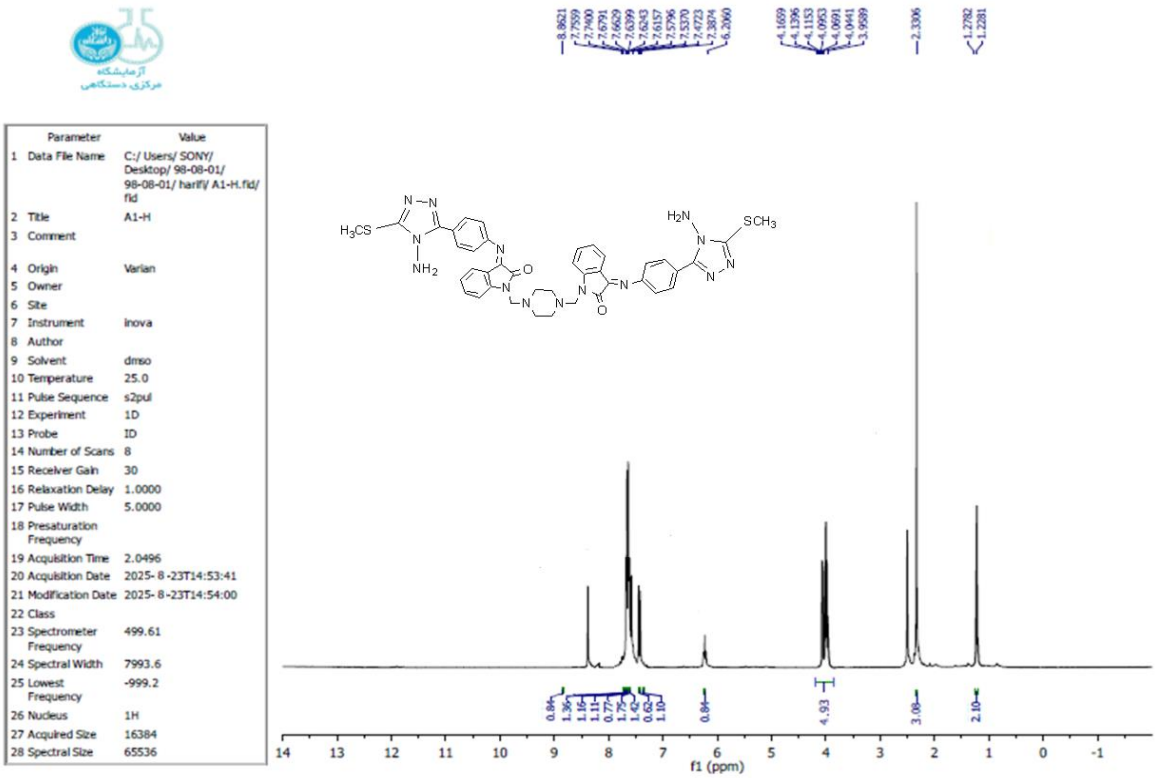

Figure 5. ^{1}H-NMR spectrum of derivative A1.

Iraqi journal of Bioscience and Biomedical
Published Online First: 31/December/2025
p-ISSN: 3007-5491 / e-ISSN:3007-5505

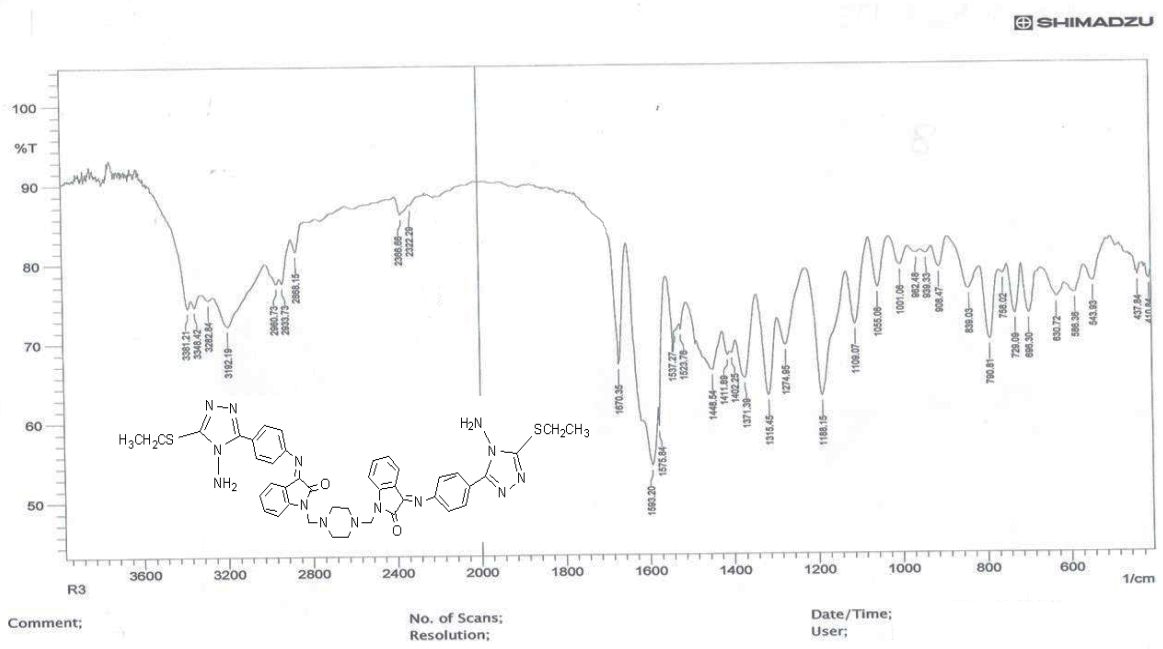

Figure 6. FTIR spectrum of derivative A2.

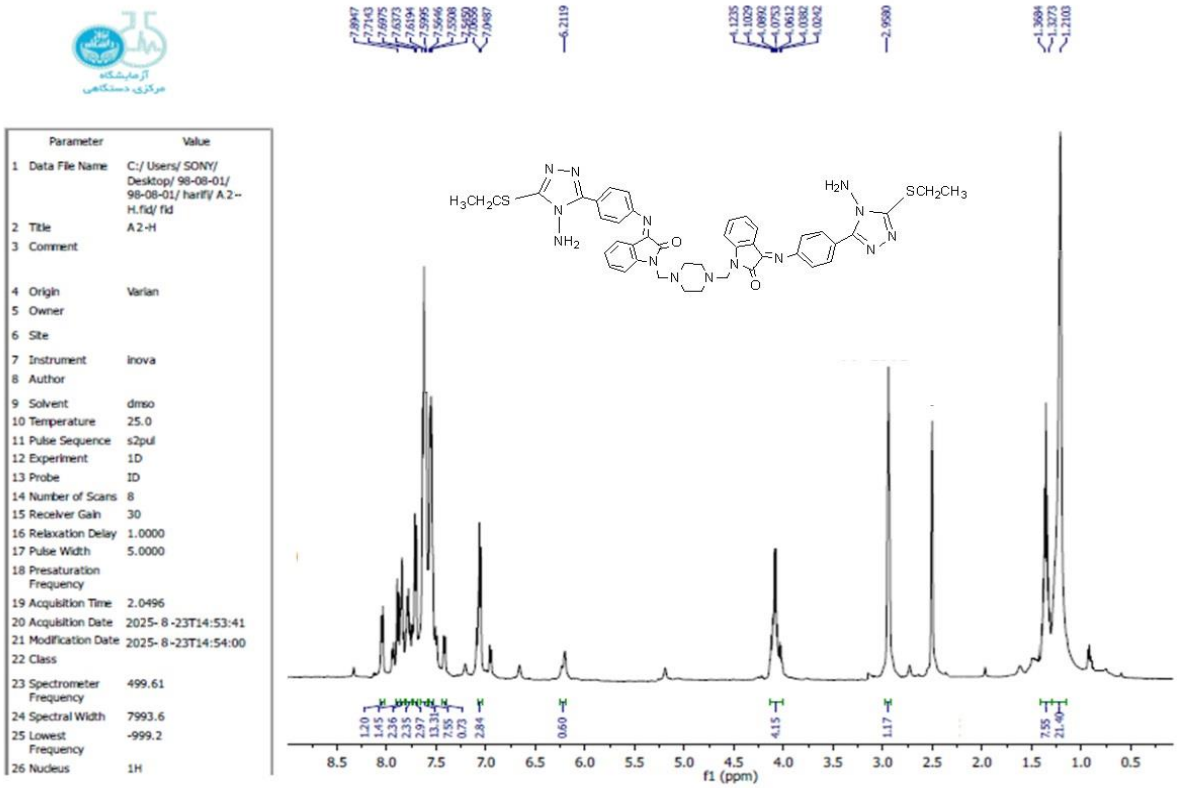

Figure 7. ^{1}H-NMR spectrum of derivative A2.

Iraqi journal of Bioscience and Biomedical
Published Online First: 31/December/2025
p-ISSN: 3007-5491 / e-ISSN:3007-5505

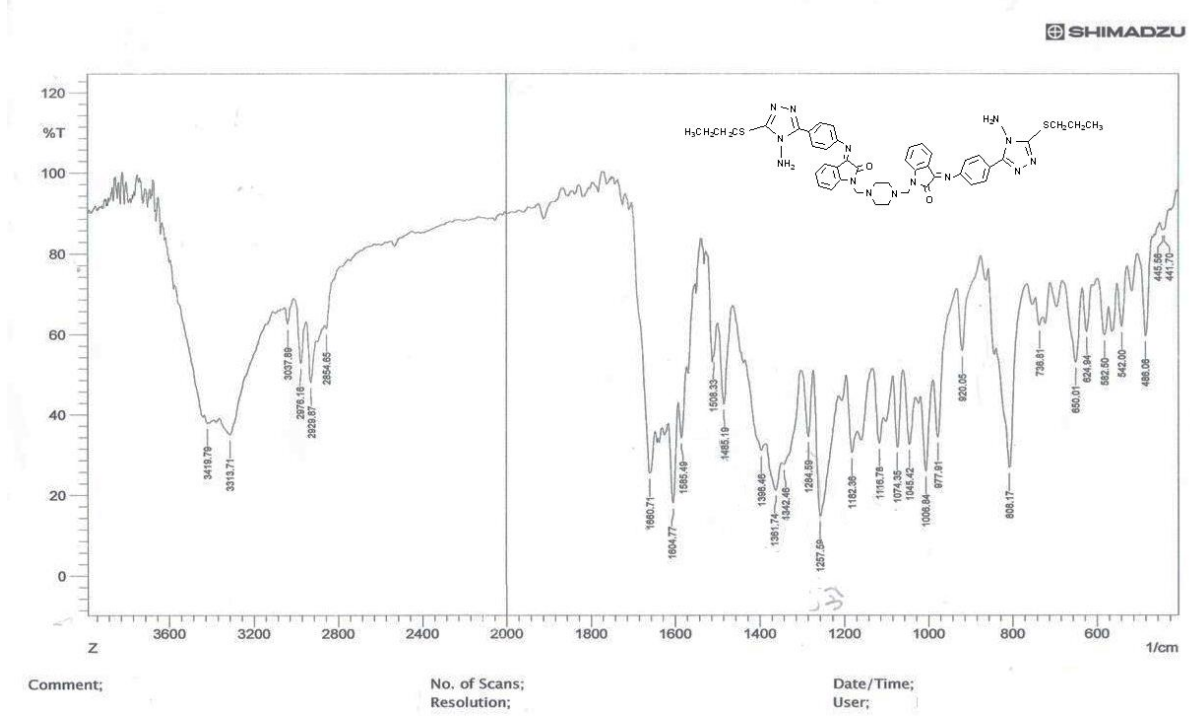

Figure 8. FTIR spectrum of derivative A3.

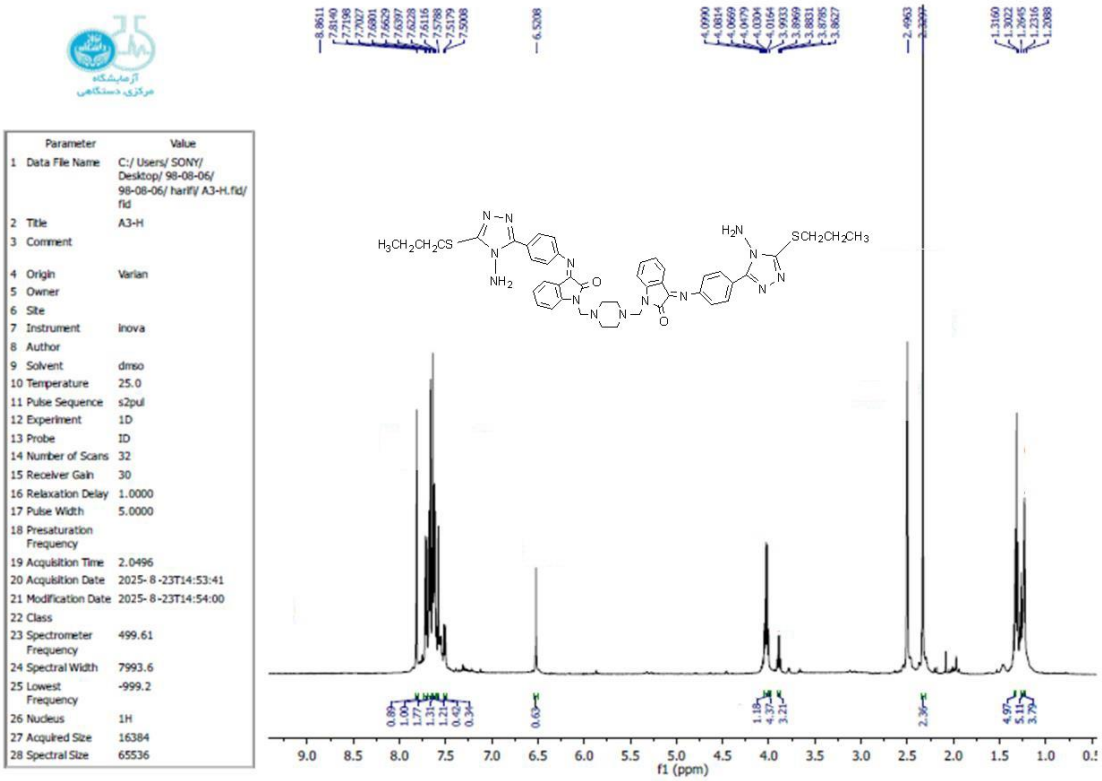

	Parameter	Value
1	Data File Name	C:/ Users/ SONY/ Desktop/ 98-08-06/ 98-08-06/ harif/ A3-H.fid/ fid
2	Title	A3-H
3	Comment	
4	Origin	Varian
5	Owner	
6	Site	
7	Instrument	Inova
8	Author	
9	Solvent	dmso
10	Temperature	25.0
11	Pulse Sequence	s2pul
12	Experiment	1D
13	Probe	ID
14	Number of Scans	32
15	Receiver Gain	30
16	Relaxation Delay	1.0000
17	Pulse Width	5.0000
18	Presaturation Frequency	
19	Acquisition Time	2.0496
20	Acquisition Date	2025- 8 -23T14:53:41
21	Modification Date	2025- 8 -23T14:54:00
22	Class	
23	Spectrometer Frequency	499.61
24	Spectral Width	7993.6
25	Lowest Frequency	-999.2
26	Nucleus	1H
27	Acquired Size	16384
28	Spectral Size	65536

Figure 9. ^{1}H-NMR spectrum of derivative A3.

Iraqi journal of Bioscience and Biomedical
Published Online First: 31/December/2025
p-ISSN: 3007-5491 / e-ISSN:3007-5505

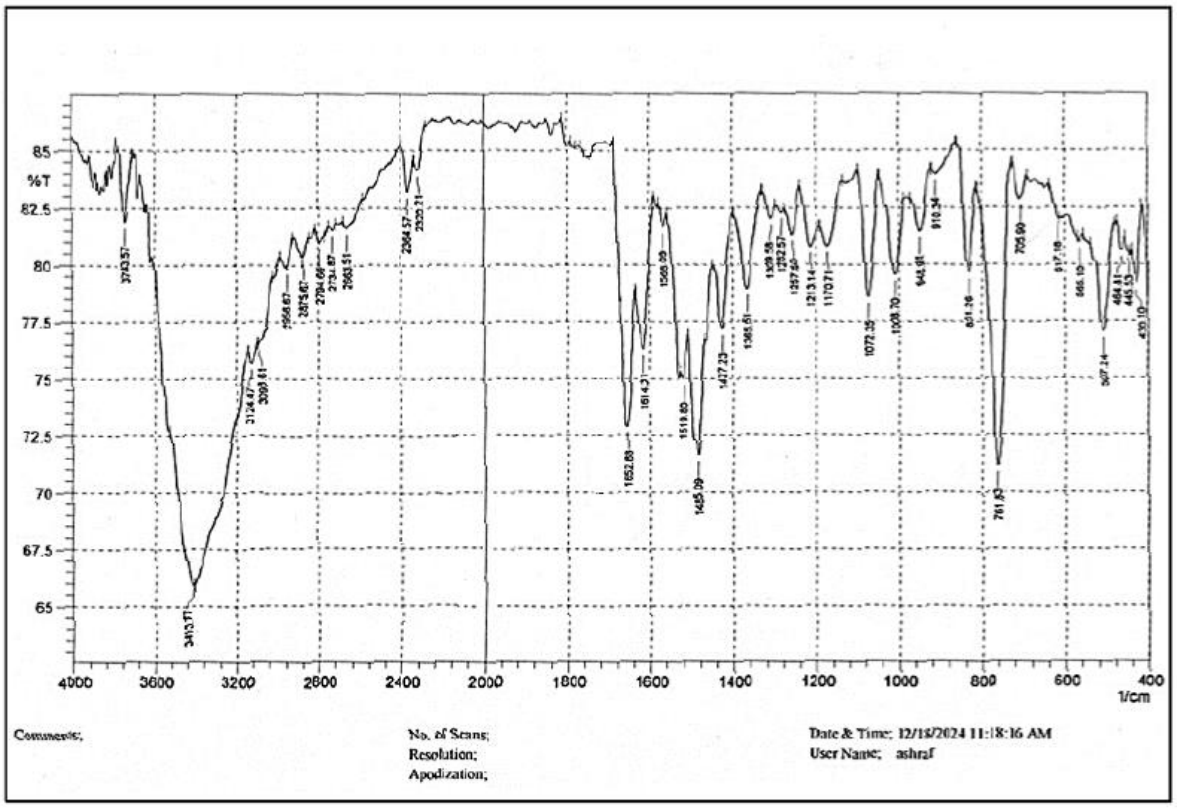

Figure 10. FTIR spectrum of derivative F.

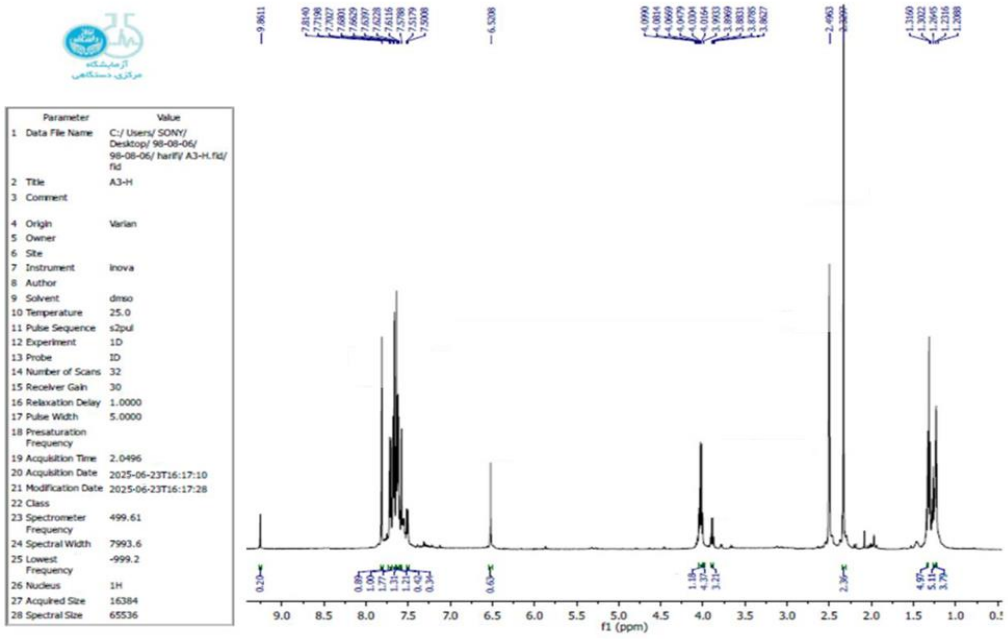

Figure 11. ^{1}H-NMR spectrum of derivative F.

Iraqi journal of Bioscience and Biomedical
Published Online First: 31/December/2025
p-ISSN: 3007-5491 / e-ISSN:3007-5505

Applications

Molecular Docking

Molecular docking serves as a key approach in the drug discovery process. In this study, MOE software was used to perform docking simulations and predict the binding modes of the synthesized compounds (A1, A2, A3, F) with the target protein (PDB ID: 3O2F) (Figure 12). The predicted binding affinities and docking scores are summarized in Table 1.

The 2D and 3D interaction profiles of the compounds with the amino acid residues of 3O2F are shown in the following figures and tables. Compounds A1, A2, A3, and F demonstrated favorable binding affinities (Table 2, Table 3). The docking analysis revealed that their interactions include hydrogen bonding and hydrophobic contacts. Bond lengths and hydrogen bond details within the active site are illustrated in the subsequent figures. Results indicate that the compounds interact with distinct amino acid residues through H-donor, H-acceptor, and H-pi contacts, in addition to multiple H-acceptor and pi-H interactions involving water molecules and protein residues. Interaction distances and binding energies are provided in Table 2.

Table 1: The binding affinity and rmsd result of 3O2F protein from docking process.

Compounds	mseq	Binding Affinity Kcal/mol	Rmsd (Å)	E_conf	E_place	E_score1	E_refine	E_score2
A1-pose1	1	-7.54431	2.176008	200.7568	17.01836	-6.90036	-16.9584	-7.54431
A1-pose2	1	-6.86691	3.278764	246.8782	61.83091	-8.85942	18.24617	-6.86691
A1- pose3	1	-6.79861	4.297086	198.8663	3.72971	-9.54315	-5.46558	-6.79861
A1- pose4	1	-5.68965	2.922421	292.1812	-0.86124	-8.24685	19.81644	-5.68965
A1- pose5	1	-5.61583	2.935867	313.578	-1.43155	-10.8605	36.63228	-5.61583
A2- pose1	2	-7.88338	2.027753	198.2906	9.627593	-8.31794	-22.4561	-7.88338
A2- pose2	2	-6.90511	4.752905	205.4846	54.18816	-6.95922	-2.87728	-6.90511
A2- pose3	2	-6.29339	2.146429	292.9289	22.0228	-7.08273	36.95395	-6.29339
A2- pose4	2	-5.68711	5.285532	291.6948	40.55624	-6.78297	45.23048	-5.68711
A2- pose5	2	-5.31633	3.446741	318.7002	34.43409	-7.27545	49.16726	-5.31633
A3- pose1	3	-8.09171	2.087459	248.2411	77.96203	2.071748	-27.84	-8.09171
A3- pose2	3	-7.67171	4.633854	269.5835	179.2993	1.648112	-14.8659	-7.67171
A3- pose3	3	-6.13511	3.121633	258.1841	79.49075	0.980284	-5.47942	-6.13511

Iraqi journal of Bioscience and Biomedical
Published Online First: 31/December/2025
p-ISSN: 3007-5491 / e-ISSN:3007-5505

A3- pose4	3	-6.98296	3.418971	321.8939	139.8026	-0.48521	97.92606	-6.98296
A3- pose5	3	-5.05400	6.746004	316.8061	96.55752	-1.72044	100.671	-5.05400
F- pose1	4	-8.69221	3.630429	260.6179	55.69045	-7.72493	-29.9131	-8.69221
F- pose2	4	-7.64913	3.831368	251.6376	47.1488	-3.17598	-12.4267	-7.64913
F- pose3	4	-7.74632	2.696581	326.5702	178.288	-1.37734	79.6919	-7.74632
F- pose4	4	-6.03651	2.238913	388.755	134.0074	-3.48443	132.5429	-6.03651
4- pose5	4	-9.23003	1.998303	373.8771	57.80422	-0.65562	190.1466	-9.23003
Standard	std	-7.17255	2.144093	-42.7381	-9.57956	-7.82319	4.316677	-7.17255

Table 2: Details of the best poses of ligands (A1, A2, A3, F) with protein $3O_2F$.

Compounds	Binding Affinity Kcal/mol	Rmsd (Å)	Atom of compound	Atom of Receptor	Involved receptor residues	Type of interaction bond	Distance (Å)	E (kcal/mol)
A1-pose1	-7.54431	2.176008	C 14 N 48	OE1 NE2	GLU 158 HIS 215	(B) H-donor (B) H-acceptor	3.14 3.15	-0.7 -1.1
A2- pose1	-7.88338	2.027753	N 57 S 58 S 58	OE1 OE1 OE2	GLU 190 GLU 190 GLU 190	(B) H-donor (B) H-donor (B) H-donor	3.60 3.81 3.53	-0.7 -0.7 -0.6
A3- pose1	-8.0917	2.087459	N 54 N 54 O 23 5-ring	O O NZ CB	ASN 107 HOH 60 LYS 114 ASN 107	(B) H-donor (B) H-donor (B) H-acceptor (B) pi-H	3.00 3.10 2.74 4.69	-1.1 -1.0 -8.5 -1.2
F- pose5	-9.23003	1.998303	S 54 S 55 5-ring	OD2 O ND2	ASP 149 LYS 114 ASN 162	(B) H-donor (B) H-donor (B) pi-H	3.61 3.29 3.32	-1.6 -3.8 -0.7
Standard	-7.17255	2.144093	N9 10 N11 13 N11 13 N5 5	O OD2 O O	HOH 365 ASP 149 HOH 60	(B) H-donor (B) H-donor (B) H-donor	2.85 2.84 3.32 2.90	-4.3 -8.4 -0.3 -1.8

Iraqi journal of Bioscience and Biomedical
Published Online First: 31/December/2025
p-ISSN: 3007-5491 / e-ISSN:3007-5505

			N11 13	OD2	HOH 391 ASP 149	(B) H-acceptor (B) ionic	2.84	-5.6

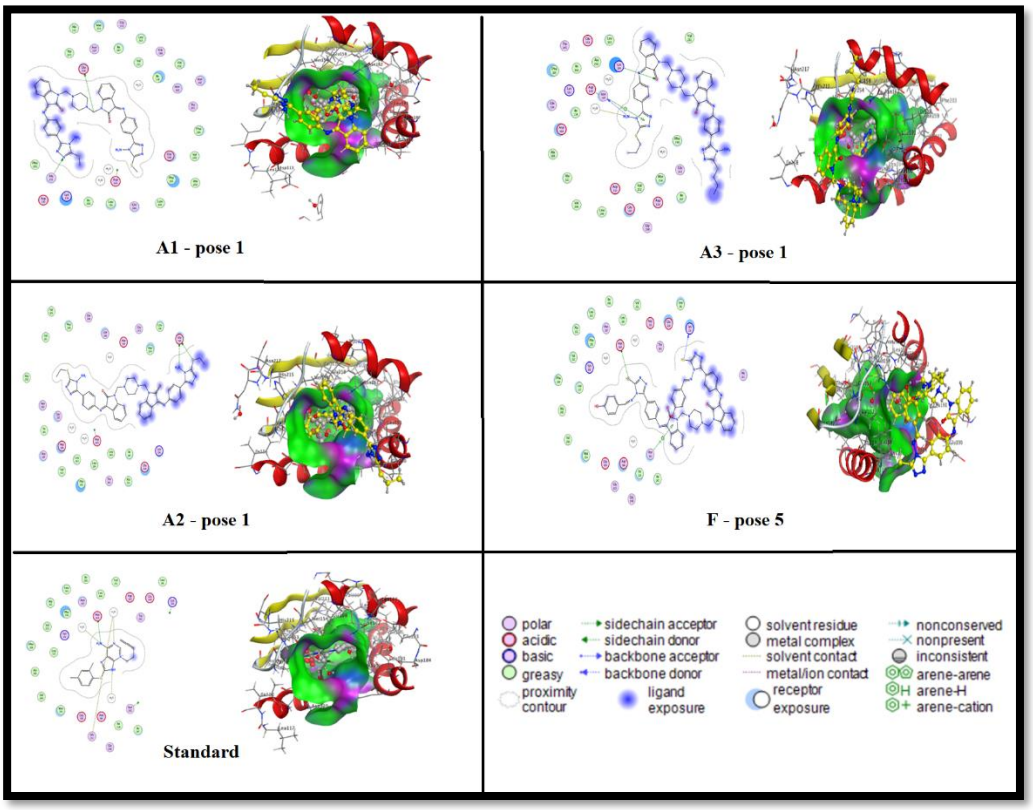

Figure 12: 2D and 3D of the best poses obtained by MOE.

Interpretation of molecular docking results

The molecular docking analysis of the compounds A1, A2, A3, and F against the $3O_2F$ protein, with PU-H54 as the standard ligand, reveals remarkable differences in binding performance, interaction profiles, and docking energetics that clearly distinguish the best candidate for protein inhibition. Looking first at binding affinity, which is the key indicator of ligand–receptor interaction strength, the results demonstrate that all four test compounds outperformed PU-H54. The best pose of compound F, identified as F-pose5, exhibited the most favorable binding affinity, reaching –9.23003 kcal/mol, a value that significantly surpasses the standard's –7.17255 kcal/mol. The next best performer was A3-pose1, which also showed strong binding at –8.0917 kcal/mol, followed by A2-pose1 at –7.88338 kcal/mol and A1-pose1 at –7.54431 kcal/mol, all of which were better than the reference ligand. This trend immediately suggests that the new compounds form more stable and energetically favorable complexes within the active site of 3O2F compared to PU-H54.

Iraqi journal of Bioscience and Biomedical
Published Online First: 31/December/2025
p-ISSN: 3007-5491 / e-ISSN:3007-5505

Examining the RMSD values, which reflect the structural accuracy and reliability of the docked pose, all of the best poses for the test compounds showed values near or slightly below 2 Å, with F-pose5 presenting the lowest RMSD at 1.998 Å, A3-pose1 at 2.087 Å, A2-pose1 at 2.027 Å, and A1-pose1 at 2.176 Å. PU-H54's best pose had a comparable RMSD of 2.144 Å, confirming that all selected ligand orientations are consistent and well accommodated in the binding pocket.

Deeper energy study reveals numerous important differences. The conformational energy (E_conf) was greatest in F-pose5, indicating a major ligand rearrangement to suit the protein location. After docking, binding affinity and refinement energies were significantly favorable, offsetting this internal strain. For the other test compounds, A3-pose1 and A2-pose1 likewise had significant E_conf values, showing binding flexibility. In contrast, PU-H54 required almost no conformational adjustment, as shown by its much lower E_conf value, but this resulted in a less effective final binding, showing that lower strain does not always indicate better binding if the ligand fails to make deeper or greater specific

The new compounds outperform PU-H54 in placement and refinement energy (E_place and E_refine). F-pose5 has a refinement energy of 190.1466, above the standard and showing a stable binding mode following minimization. Instead of PU-H54's poor E_refine score, A3-pose1 and A2-pose1 performed well. These data show that the test drugs attach tightly and optimize docking contact better than the standard.

The comprehensive interaction study between each ligand and the 3O2F binding pocket amino acid residues may provide the most important discoveries. Two hydrogen bonds—one donor with GLU 158 and one acceptor with HIS 215—moderately stabilized A1-pose1. A2-pose1 established three hydrogen connections with GLU 190, each increasing stabilizing energy but not much. A3-pose1 has a diverse interaction profile, including two hydrogen bonds with ASN 107 and HOH 60, a strong hydrogen bond acceptor with LYS 114, and a π–H interaction with ASN 107, enhancing binding by aromatic stacking. The strong hydrogen bond with LYS 114, with an energy of –8.5 kcal/mol and a distance of 2.74 Å, contributes to A3's exceptional performance. F-pose5 has the strongest interaction network, forming hydrogen bonds with ASP 149 and LYS 114 and a π–H interaction with ASN 162, all with distances under 3.6 Å and energies that provide exceptional stabilization. F has several interaction types and large cumulative binding energies, making it the most strongly bound ligand in this class.

The typical ligand PU-H54 is well-accommodated in the pocket with a decent RMSD and moderate internal strain, but its network of contacts is modest and less energetically relevant. The majority of its energy comes from hydrogen bonding with water molecules (HOH 365, HOH 60, HOH 391) and ASP 149, with just one moderately strong ionic connection and fewer direct interactions with important protein residues. The strongest interaction for PU-H54 with ASP 149 is –8.4 kcal/mol, close to A3's best but lacks the reinforcement from numerous concurrent interactions that F and A3's greatest postures have.

Taken together, the docking data and interaction analysis leave little doubt that compound F, especially in its pose5 orientation, is the most promising inhibitor among all those studied here, showing the highest binding affinity, the most favorable refinement energy, excellent geometric fit, and a diverse

Iraqi journal of Bioscience and Biomedical
Published Online First: 31/December/2025
p-ISSN: 3007-5491 / e-ISSN:3007-5505

and strong network of specific ligand–protein interactions. A3 also emerges as an excellent candidate due to its similarly strong affinity and exceptional hydrogen bonding with LYS 114. Although exceeding PU-H54 in affinity and post-docking energies, A1 and A2 fall behind F and A3 in binding relationship richness and strength. Since molecules F and A3 outperformed the natural ligand PU-H54 in binding energy and interaction profile, they justify further biological research as 3O2F protein inhibitors.

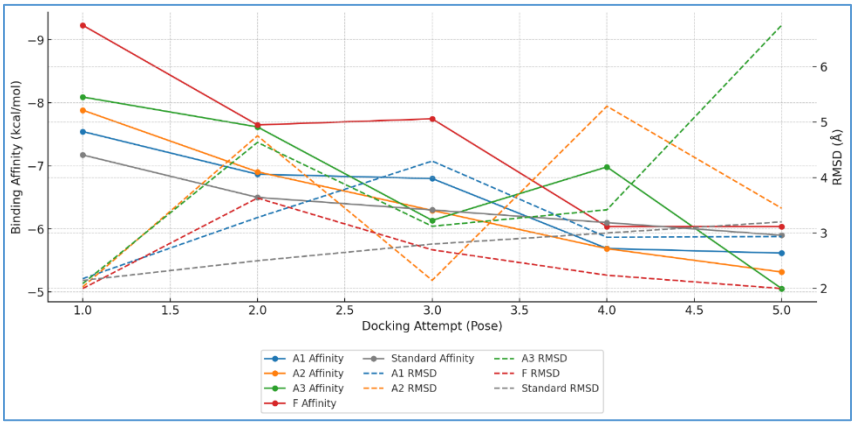

Figure 13. Binding affinity (solid lines) and RMSD (dashed lines) for each of the derivatives (A1, A2, A3, F, and the standard ligand PU-H54).

Figure 13 shows the binding affinity (solid lines) and RMSD (dashed lines) for derivatives A1, A2, A3, F, and the reference ligand PU-H54 in the five optimal docking postures with the 3O2F protein. The left Y-axis shows binding affinity in kcal/mol. Lower values imply greater ligand-protein binding. The right Y-axis displays RMSD values in Ångströms, indicating docking posture stability and dependability. Lower values suggest a more consistent fit. The data reveals that compound F has the highest binding affinity, followed by A3 and the conventional ligand PU-H54. RMSD values vary by chemical and posture, revealing each ligand's consistency and location in the protein's binding pocket. This visualisation instantly shows which chemicals bind stronger and dock more stablely than the standard reference.

Anti-breast cancer MCF-7 cell line

Mannich base derivatives have several pharmacological uses, including anticancer activity. This research examines the cytotoxic effects of three manufactured Mannich derivatives, A1, A2, and A3, on MCF-7 human breast cancer cells after 24 hours. Cell viability is measured from 0 to 320 ppm and IC50 values are calculated to compare potency. High-activity derivative A1 reduces viability from 100.0% at 0 ppm to 7.84% at 320 ppm with an IC50 of 100 ppm. Derivative A2 inhibits much more with an IC50 of 294.07 ppm, reducing from 99.46% to 11.10%. Derivative A3 has a weaker IC50 of 294.07 ppm, sustaining over 50% viability till 80 ppm and 12.08% at 320 ppm. Differential interactions with cellular targets imply that derivatives A1 and A2 are better prospects for continued development, whereas derivative 3 may need structural modification or combination tactics. Comparative findings support prioritizing Mannich compounds in breast cancer therapy research.

Iraqi journal of Bioscience and Biomedical
Published Online First: 31/December/2025
p-ISSN: 3007-5491 / e-ISSN:3007-5505

Table 4: Derivative (A1)-induced MCF-7 cell viability.

Concentration (PPM)	After 24 h	
	Mean	±SD
0	100	2.218342
20	61.53055	2.392601
40	50.71383	2.954389
80	34.53698	1.923883
160	19.23794	2.16052
320	7.848875	1.214987

Derivative A1 strongly inhibits MCF-7 cell development, reducing viability from control to 34.53% at 80 ppm and 7.84% at 320 ppm. An IC50 of 41.23 ppm indicates significant potency. The fast viability loss between 20 and 80 ppm supports binding to proliferation-regulating cellular sites. This pattern matches Mannich bases with aromatic substituents, which alter mitochondrial function to cause apoptosis in estrogen receptor-positive breast cancer cells (Table 4 and Figures 14 and 15).

Similar Mannich compounds have shown MCF-7 cell cytotoxicity at sub-100 ppm IC50 values. M. H. Abdelrahman and M. M. Ali (2016) found comparable structural patterns with IC50 values between 35 and 60 ppm [25].

Table 5: Derivative (A2)-induced MCF-7 cell viability.

Concentration (PPM)	After 24 h	
	Mean	±SD
0	99.46302	2.150476
20	79.07074	2.096579
40	67.67846	2.49011
80	52.05466	1.318842
160	33.18971	2.155821
320	11.10611	2.147258

Derivative A2 yields an IC50 of 86.25 ppm, with viability decreasing steadily from 79.07% at 20 ppm to 33.18% at 160 ppm and 11.10% at 320 ppm. Although less powerful than derivative A1, its inhibitory profile is constant across dosages, suggesting steady growth-regulating protein interaction. As demonstrated in Table 5 and Figures 16 and 17, Mannich compounds of moderate lipophilicity have dose–response curves that maintain cytotoxic effect across a wide concentration range.

Iraqi journal of Bioscience and Biomedical
Published Online First: 31/December/2025
p-ISSN: 3007-5491 / e-ISSN:3007-5505

Yamali, C., Gul, M., & Gul, H. I. (2023) found comparable steady inhibitory patterns in Mannich derivatives with IC50 values of 70–100 ppm [26]. Khan et al. found that substituents influencing electron density on the amine-linked aromatic ring significantly affect cytotoxic activity [27]. These derivatives often inhibit topoisomerase II, reducing DNA replication efficiency in cancer cells. Literature also emphasizes that consistent cytotoxicity over multiple concentrations is advantageous for maintaining therapeutic effects under fluctuating plasma drug levels *in vivo*.

Table 6: Derivative (A3)-induced MCF-7 cell viability.

Concentration (PPM)	After 24 h	
	Mean	±SD
0	99.82637	1.822139
20	75.00322	1.028421
40	62.33119	1.727586
80	49.17363	2.234162
160	31.01929	1.388945
320	12.08039	2.575225

Although derivative A3 has the lowest potency (IC50 = 76.57 ppm), it nevertheless has above 50% survivability till 80 ppm. Delaying inhibition implies poorer affinity for cancer cell targets or less cellular uptake. Despite lesser potency, the dramatic drop to 12.08% viability at 320 ppm shows that greater dosages may still be harmful (Table 6 and Figures 16 and 17).

Iraqi journal of Bioscience and Biomedical
Published Online First: 31/December/2025
p-ISSN: 3007-5491 / e-ISSN:3007-5505

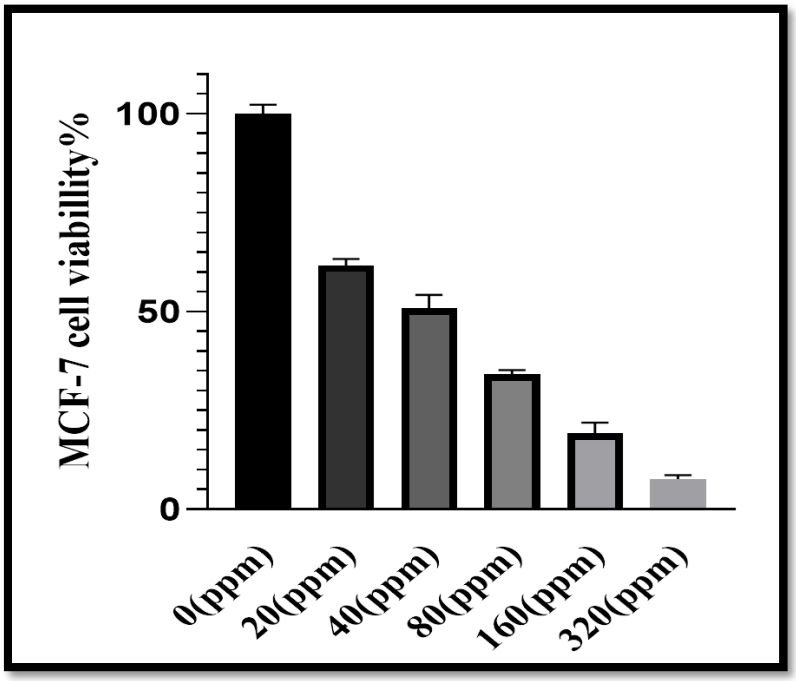

Figure 14. Effect of derivative A1 on MCF-7 cell viability %.

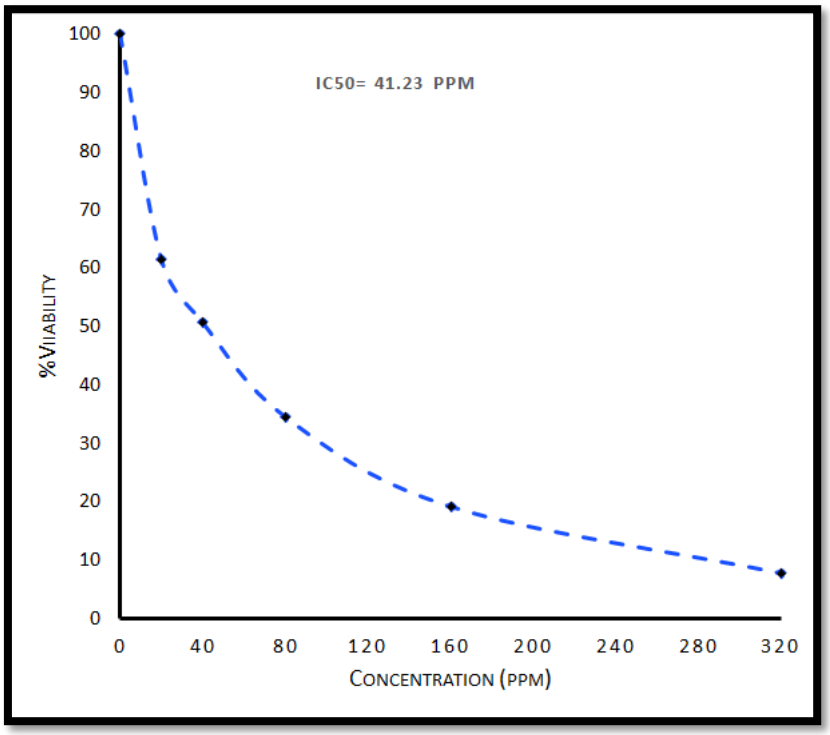

Figure 15. IC50 of derivative A1 on MCF-7 cell viability %.

Iraqi journal of Bioscience and Biomedical
Published Online First: 31/December/2025
p-ISSN: 3007-5491 / e-ISSN:3007-5505

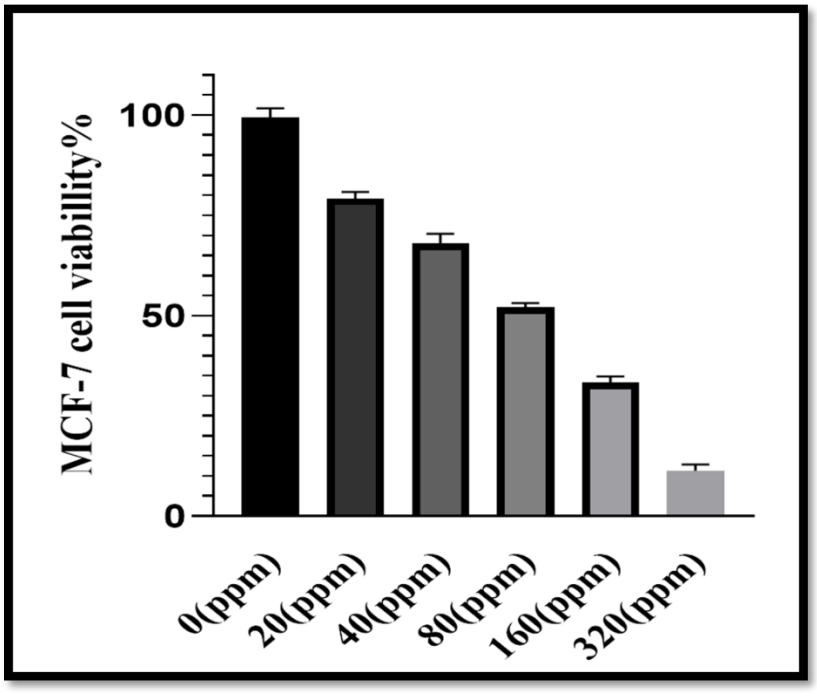

Figure 16. IC50 of derivative A2 on MCF-7 cell viability %.

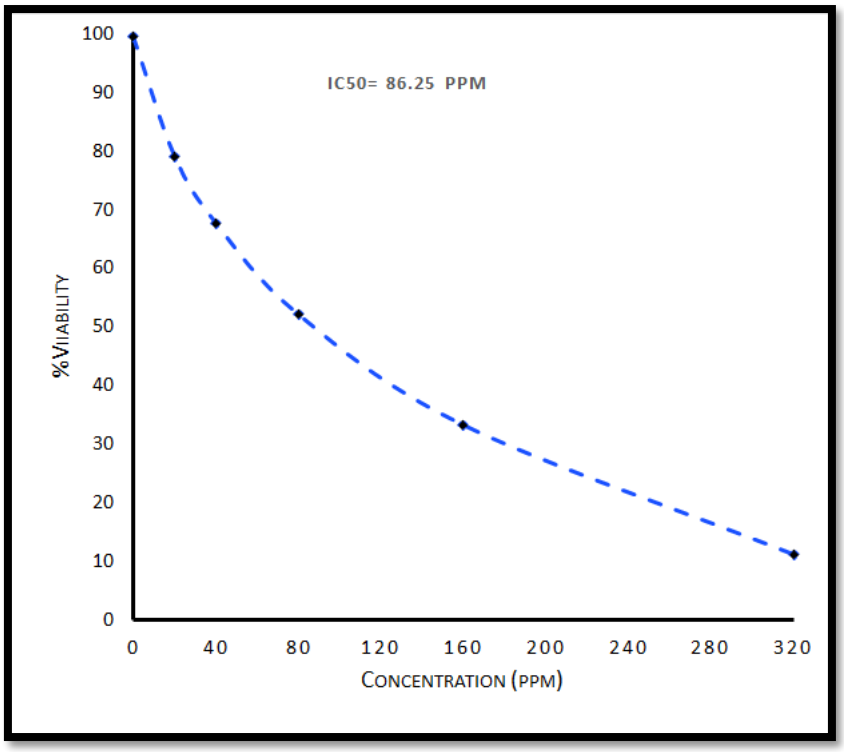

Figure 17. IC50 of derivative A2 on MCF-7 cell viability %.

Iraqi journal of Bioscience and Biomedical
Published Online First: 31/December/2025
p-ISSN: 3007-5491 / e-ISSN:3007-5505

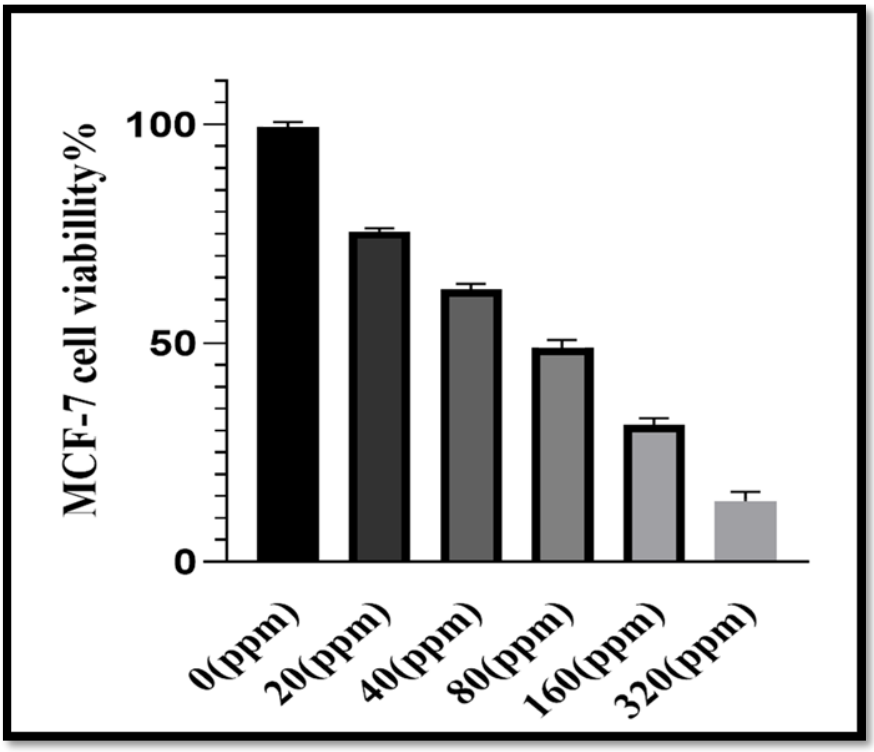

Figure 18. IC50 of derivative A3 on MCF-7 cell viability %.

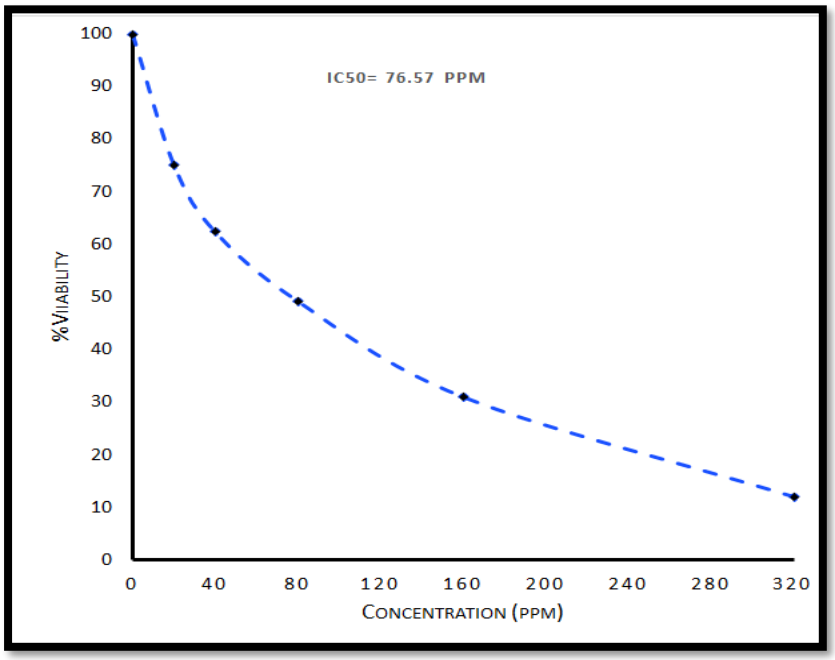

Figure 19. IC50 of derivative A3 on MCF-7 cell viability %.

Iraqi journal of Bioscience and Biomedical
Published Online First: 31/December/2025
p-ISSN: 3007-5491 / e-ISSN:3007-5505

Studies on Mannich derivatives with bulky or polar substituents have reported similar delayed inhibition effects, as described by Subramaniapillai, S. G. (2013), where steric hindrance lowered receptor binding rates [28]. Strzelecka, M. (2022), have indicated that such compounds remain valuable in combination therapy, where synergistic interactions reduce the required dose [29].

Conclusion

Molecular docking analysis showed that all derivatives had stronger binding affinities than PU-H54, with compound F being the most potent binder (–9.23 kcal/mol) due to multiple hydrogen bonds and π–H interactions, ensuring high stability in the active pocket. Strong affinity and extensive interaction patterns supported Compound A3's inhibitor potential. Cytotoxicity testing on MCF-7 breast cancer cells showed significant antiproliferative effects for derivatives 1 and 2, with IC_{50} values of 41.23 ppm and 86.25 ppm, respectively. Derivative 3 showed weaker potency but still showed inhibitory action at higher concentrations. These findings demonstrate how Mannich alteration improves triazole-based scaffold solubility, binding affinity, and biological activity.

Acknowledgment

We thank the Chemistry Department, College of Science, Al-Nahrain University.

Authors' Declaration

- We hereby confirm that all the Figures in the manuscript are original and have been created by us.
- We have obtained ethical clearance for our study from the local ethical committee at [Al-Nahrain University]. This approval underscores our commitment to ethical research practices and the well-being of our participants.

Authors' Contribution Statement

Wahad K. Kareem[1]: Collect and write a review.

Nasreen R. Jber[2] and Ahmed Al-Ani[3]: Design and supervisor of a review.

References

1 Jangir, N., Poonam, Dhadda, S. & Jangid, D. K. Recent advances in the synthesis of five-and six-membered heterocycles as bioactive skeleton: A concise overview. *ChemistrySelect* **7**, e202103139 (2022).

2 YÜCEL, T. B. SYNTHESIS OF TRIAZOLE DERIVATIVE COMPOUNDS AND THEIR IMPORTANCE IN PHARMACOLOGY. *SCIENCE AND MATHEMATICS*, 133 (2023).

3 Guan, Q. *et al.* Triazoles in medicinal chemistry: physicochemical properties, bioisosterism, and application. *Journal of Medicinal Chemistry* **67**, 7788-7824 (2024).

4 Flieger, S. *Design and Synthesis of Novel Antibiotics and Anticancer Agents Targeting Pharmaceutically Relevant Enzymes*, Loyola University Chicago, (2023).

5 Alam, M. M. 1, 2, 3-Triazole hybrids as anticancer agents: A review. *Archiv der Pharmazie* **355**, 2100158 (2022).

6 Raman, A. P. S. *et al.* An updated review on 1, 2, 3-/1, 2, 4-triazoles: synthesis and diverse range of biological potential. *Molecular Diversity* **29**, 899-964 (2025).

7 Sumrra, S. H., Zafar, W., Imran, M. & Chohan, Z. H. A review on the biomedical efficacy of transition metal triazole compounds. *Journal of Coordination Chemistry* **75**, 293-334 (2022).

8 Liang, T., Sun, X., Li, W., Hou, G. & Gao, F. 1, 2, 3-Triazole-containing compounds as anti–lung cancer agents: Current developments, mechanisms of action, and structure–activity relationship. *Frontiers in pharmacology* **12**, 661173 (2021).

9 Juaila, K. M. & Jber, N. R. Synthesis, Characterization and Evaluation of the Antimicrobial Activity of a New [1, 2, 4] Triazolo [3, 4-B][1, 3, 4] Thiadiazoles Derivatives. *Al-Nahrain Journal of Science* **27**, 1-8 (2024).

10 Abood, R. G. *et al.* Anti-breast cancer potential of new indole derivatives: Synthesis, in-silico study, and cytotoxicity evaluation on MCF-7 cells. *Journal of Molecular Structure* **1326**, 141176 (2025).

11 Sachdeva, H., Saquib, M. & Tanwar, K. Design and development of triazole derivatives as prospective anticancer agents: a review. *Anti-Cancer Agents in Medicinal Chemistry-Anti-Cancer Agents)* **22**, 3269-3279 (2022).

12 Javaheri, F. H. H., Ghafouri, H. & Piravar, Z. The cytotoxic effects of a bioactive nitro derivative of pyrimidine to human breast cancer (MCF-7) cells. *Journal of Biological Studies* **5**, 113-119 (2022).

13 Othmène, Y. B. *et al.* Triazole fungicide tebuconazole induces apoptosis through ROS-mediated endoplasmic reticulum stress pathway. *Environmental Toxicology and Pharmacology* **94**, 103919 (2022).

14 Molani Gol, R. & Kheirouri, S. The effects of quercetin on the apoptosis of human breast cancer cell lines MCF-7 and MDA-MB-231: A systematic review. *Nutrition and Cancer* **74**, 405-422 (2022).

15 Quiroga, D. & Coy-Barrera, E. Synthesis of antifungal heterocycle-containing Mannich bases: A comprehensive review. *Organics* **4**, 503-523 (2023).

16 Yadav, M. K. & Chowdhury, S. Recent advances in the electrochemical functionalization of N-heterocycles. *Organic & Biomolecular Chemistry* (2025).

17 Luong, L. Q. & Vu, T. K. Coumarin-derived Mannich bases: a review of biological activities. *Letters in Organic Chemistry* **21**, 303-319 (2024).

18 Al-Khazraji, A. M. A. Synthesis, Characterization, and Evaluation of MCF-7 (Breast Cancer) for Schiff, Mannich Bases, and Their Complexes. *Indonesian Journal of Chemistry* **24**, 213-227 (2024).

19 Mukhlif, M. M. & Al-Mudhafar, M. M. J. Synthesis, characterization, and preliminary antimicrobial evaluation of new Schiff bases and Mannich bases of isatin. *Iraqi Journal of Pharmaceutical Sciences* **32**, 156-163 (2023).

20 Abbas, A. K. & Jber, N. R. Synthesis and Characterization of New Oxazepine Compounds and Estimation its Biological Activity. *Al-Nahrain Journal of Science* **23**, 17-23 (2020).

21 Amin, N. H., El-Saadi, M. T., Ibrahim, A. A. & Abdel-Rahman, H. M. Design, synthesis and mechanistic study of new 1, 2, 4-triazole derivatives as antimicrobial agents. *Bioorganic chemistry* **111**, 104841 (2021).

22 Kapp, J. D., Green, R. E. & Shapiro, B. A fast and efficient single-stranded genomic library preparation method optimized for ancient DNA. *Journal of Heredity* **112**, 241-249 (2021).

23 Magni, A. *et al.* N-Glycosylation-Induced Pathologic Protein Conformations as a Tool to Guide the Selection of Biologically Active Small Molecules. *Chemistry–A European Journal* **30**, e202401957 (2024).

24 Dernovšek, J. & Tomašič, T. Following the design path of isoform-selective Hsp90 inhibitors: small differences, great opportunities. *Pharmacology & therapeutics* **245**, 108396 (2023).

25 Abdelrahman, M. H. & Ali, M. M. Synthesis of novel pyrazole derivatives bearing 1, 2, 4-triazole moiety as potential anticancer agents. *Bulletin of Pharmaceutical Sciences Assiut University* **39**, 53-71 (2016).

26 Yamali, C., Gul, M. & Gul, H. I. Current pharmaceutical research on the significant pharmacophore mannich bases in drug design. *Current Topics in Medicinal Chemistry* **23**, 2590-2608 (2023).

27 Khurshid, M. *et al.* Bacterial munch for infants: potential pediatric therapeutic interventions of probiotics. *Future microbiology* **10**, 1881-1895 (2015).

28 Subramaniapillai, S. G. Mannich reaction: A versatile and convenient approach to bioactive skeletons. *Journal of Chemical Sciences* **125**, 467-482 (2013).

29 Strzelecka, M. *et al.* Synthesis, anticancer activity and molecular docking studies of novel N-Mannich bases of 1, 3, 4-oxadiazole based on 4, 6-dimethylpyridine scaffold. *International Journal of Molecular Sciences* **23**, 11173 (2022).